Advances in Nano Research, *Vol. 18, No. 3 (2025) 289-298*
https://doi.org/10.12989/anr.2025.18.3.289

The effect of smart nanoparticles on the computational optimization of beams using cloud-based framework for computer simulation

Hui Li[1], Chenxia Wu[1], Yao Lu[1], Hongqiao Yan[*1] and M. Kaffashi[2]

[1]*School of Sport Communication and Information Technology, Shandong Sport University, Jinan 250000, Shandong, China*
[2]*Department of Civil Engineering, University of Zabol, Zabol, Iran*

(*Received April 17, 2024, Revised March 6, 2025, Accepted March 6, 2025*)

Abstract. The study evaluates how smart nanoparticles affect beam structural performance while using computational resources hosted on remote servers. An enhanced advanced adaptive harmony search algorithm (AAHS) serves to boost optimization efficiency levels. The algorithm makes two sequential parameter adjustment stages which start by adapting harmony memory through variable bandwidth methods and proceed with adaptive step-size implementations. The research investigates the best design parameters for ZnO nanoparticle reinforced nanocomposite sinusoidal beams under different axial force and foundation property conditions and applied voltage levels. Results show that the proposed AAHS method outperforms alternative optimization methods according to comparative research. Under 50 GPa buckling force and 100 V applied voltage the optimal beam should have L/h ratio of 4.425 together with 118 GPa foundation spring constant, 29 Pa shearing constant and 0.055 ZnO nanoparticle volume fraction. The study demonstrates that all three factors namely applied voltage, buckling force and foundation stiffness critically affect optimization of beams.
Keywords: AAHS method; computer simulation; nanocomposite beam; optimization; smart nanoparticles

1. Introduction

Traditional optimization methods experience difficulty when dealing with high-dimensional design spaces during nanocomposite beam modeling. Cloud-based computational frameworks now present solutions that scale operations for real-time simulations along with improved accuracy while reducing calculations time. Cloud computing provides powerful capabilities to perform lengthy parametric studies that allow researchers to examine extensive material variations and multiple loading scenarios and different geometric features quickly (Kuang *et al*. 2024, Berghouti *et al*. 2023).

This paper represents the first study which solves buckling optimization problems of nanocomposite beams reinforced with ZnO nanoparticles through advanced mathematical modeling and optimization techniques. The paper uses AAHS to execute optimization on sinusoidal beams embedded with nanocomposite under buckling limitations for its first instance. The structural modeling uses SSDT for analysis while deriving equations through the energy method and Hamilton's principle and applying an exact solution to calculate buckling load. This research evaluates how optimum design conditions respond to changes in axial forces together with applied voltage and foundation shear and spring constants and ZnO nanoparticle volume fraction levels. By filling the literature void the research establishes fundamental foundations for improving nanocomposite beams and generates original findings that enhance modern structural design practices. Functionally graded sandwich structures have been the focus of multiple studies which examined their free vibration responses through parametric and uncertainty investigation. The study creates crucial understanding about dynamic system responses when observing the combination of material grading features and boundary conditions and geometrical properties (Belarbi *et al*. 2024a). The analysis of laminated sandwich plates through wavelet finite element methods has gained attention in recent times to generate more accurate vibration analysis outcomes (Sabherwal *et al*. 2024). HSDTs stand as prominent analytical methods for modeling FGM plates and beams because they successfully account for shear and normal deformations. The authors Belabed *et al*. (2014) developed a straightforward HSDT for FGM plate analysis which produced superior accuracy together with reduced computational time. The static bending analysis of functionally graded plates with different material gradient functions such as power-law, exponential, and sigmoid through advanced finite element modeling became possible (Belarbi *et al*. 2025). The addition of carbon nanotubes (CNTs) as nanomaterials to FGMs serves to increase their mechanical properties even further. The paper by Daikh *et al*. (2022) studied static and dynamic stability of multiscale CNT-reinforced FGM nanoplates by utilizing quasi-3D nonlocal strain gradient theory. Stability outcomes in their study depended directly on micro-structural relationships which the researchers showed through their work. The research directed by Daikh *et al*. (2024) presented a thickness-stretching and microstructure-dependent model for tri-directionally coated plates to study

*Corresponding author, Ph.D.,
E-mail: yanhongqiao@sdpei.edu.cn

ISSN: 2287-237X (Print), 2287-2388 (Online)

how nanoscale effects influence FGM structures. Research on sandwich curved beams with functionally graded properties concentrated on mechanical responses through refined HSDTs which resulted in better predictions of bending as well as vibration behavior (Belarbi *et al*. 2022). Researchers have developed specialized refined shear deformation theory for beam bending and free vibration assessments of FGM beams to improve theoretical studies of these structures (Khechai *et al*. 2020). Research has merged existing methods to analyze nano-isotropic structures and nano-FGM composites and CNT-reinforced nanocomposites through systematic reviews that set the foundation for further investigation (Garg *et al*. 2022). Numerical methods with advanced capabilities evaluate the bending and buckling response of FGM nanobeams as a part of their analysis. Belarbi *et al*. (2021) developed a nonlocal finite element model with a new shear deformation theory which improved the accuracy in modeling size-dependent effects. Research studies evaluated the vibrations of functionally graded sandwich nanoplates while experiencing temperature changes (Daikh *et al*. 2021). Researchers studying FGM beams have investigated the addition of porosity because of its significance in nano-composite structures. The analysis model for functionally graded porous nanocomposite beams was developed by Merzouki *et al*. (2022) through implementation of nonlocal strain gradient theory. Through their study researchers gained fundamental knowledge about how nanocomposite beam behavior changes due to different porosity distributions.

There are a number of studies on buckling behavior of composite structures. Vodenitcharova and Zhang (2006) investigated nanocomposite beams with SWCNTs based on the Airy stress-function theory. Yas and Samadi (2012) investigated buckling in SWCNT-reinforced Timoshenko beams on elastic foundations using GDQM. Mehri *et al*. (2016) investigated buckling and vibration of SWCNT-reinforced truncated conical shells under axial compression and external pressure. Nejati *et al*. (2016) investigated cantilever FG beams with CNTs. Alesadi *et al*. (2017) coupled IGA and CUF for the buckling analysis of composite plates. Yang *et al*. (2017) examined postbuckling of GPL-reinforced nanocomposite beams on elastic foundations. Each GPLRC layer contains distributed GPLs that are uniformly scattered throughout them while following random orientations regarding the thickness direction. The authors Karimian *et al*. (2018) established a multi-layer finite element model for both buckling and free vibration analysis of laminated beams following a higher-order layer-wise theory.

Research dealing with optimization design conditions of nanocomposite structures has not been investigated in the above mentioned works. Cheng *et al*. (2011) focused on developing optimized residual thermal–mechanical response simulations for the new Flip Chip (FC) technology starting from fabrication through completion. Rouhi and Rais-Rohani (2013) delivered modeling and probabilistic design optimization for buckling purposes of nanofiber-enhanced composite cylinders. The buckling force strength of hybrid laminated nanocomposite was studied by Azadi and Rostamiyan (2015) through Taguchi method while analyzing the effects of three parameters including carbon fiber orientation, nano clay and CNT wt%. The research by Horny *et al*. (2016) investigated thermal and mechanical optimization of bio-polymer nanocomposites. The study conducted by Mansour *et al*. (2016) established an effective modal testing technique for viscoelastic composite materials using analytical–experimental transfer functions coupled with genetic algorithms. This method achieved identification by minimizing measurement discrepancies between experimental test responses and theoretical calculations. The research of Zhang *et al*. (2018) examined aerothermo-elastic behavior of CNT reinforced functionally graded composite panels exposed to supersonic airflow conditions. The genetic algorithm helped identify the best placement along with size for piezoelectric patches.

The main effort of the meta-heuristic optimization algorithm is to search the global design conditions of engineering problems based on random generations of the design variables in the feasible region (Keshtegar *et al*. 2017, Ouyang *et al*. 2017). The harmony search optimization is a simple and efficient meta-heuristic algorithm, which is inspired by music improvisation process (Guo *et al*. 2016, Omran and Mahdavi 2008) a one of the meta-heuristic algorithm using modified version of harmony search for optimization of complex structural (Keshtegar *et al*. 2017), mathematical (Zou *et al*. 2011) and engineering problems (Akin and Saka 2015). The accuracy of the optimum design for applicable nonlinear engineering problems is a one of major effort of optimization algorithm to search optimum conditions (Wang *et al*. 2017). The feature selection approach for high dimensional optimization problems was proposed using self-adjusted HS. The input dataset selection for predicting the daily time series suspended sediment was applied using response surface method basis global harmony search (GHS) (Afan *et al*. 2017). The HS was improved by dual strategies and adaptive parameters to search best design conditions of mathematical optimization problems. Two adjusting steps were applied for generating the harmony memory in improved global-best harmony search, Gaussian global-best harmony search and adaptive dynamic harmony search and these improved version of HS the best numerical results compared to original harmony search. The HS is high performance for the solution space but HS algorithm may provide some drawbacks as, (1) the performance of optimization process using HS is strongly sensitive to its parameters. (2) The improvisation mechanism of HS is stochastically to search the optimal conditions but, prior knowledge is used to guide improvisation of the effectiveness of new harmony vector. The improve version of HS is proposed to improve drawbacks of the HS algorithm using two adjusting processes for new harmony memory with dynamical permeates.

This paper represents the first study which solves buckling optimization problems of nanocomposite beams reinforced with ZnO nanoparticles through advanced mathematical modeling and optimization techniques. The paper uses AAHS to execute optimization on sinusoidal beams embedded with nanocomposite under buckling

limitations for its first instance. The structural modeling uses SSDT for analysis while deriving equations through the energy method and Hamilton's principle and applying an exact solution to calculate buckling load. This research evaluates how optimum design conditions respond to changes in axial forces together with applied voltage and foundation shear and spring constants and ZnO nanoparticle volume fraction levels. By filling the literature void the research establishes fundamental foundations for improving nanocomposite beams and generates original findings that enhance modern structural design practices.

2. AAHS optimization technique

Harmony Search tracks the best solution by following five basic methods to conduct its random search (Wang *et al*. 2017).

1- Our primary step includes describing both the optimization job and HS parameter values: Phase 1 requires transforming the optimization problem into HS format while configuring its basic features.

2- Initializing harmony memory (HM): To create the harmony memory the system generates numbers based on the uniform random distribution as:

$$x \quad = x^L + r\ and() \times (x^U - x^L) \tag{1}$$

in which, $rand() \in [0,1]$ is random, x^U and x^L are the upper/lower bounds, respectively.

3-Generating a new harmony memory: The existing harmony memory goes through a random change according to the HS set parameters. This process works through:

$$x'^j_i = \begin{cases} x_i^j \text{ with probability } HMCR \\ x_i^L + r \times (x_i^U - x_i^L) \text{ with probability 1-HMCR} \end{cases} \tag{2}$$

The algorithm uses HMCR to establish the odds of drawing information from past HM sources. A bandwidth parameter (bw) performs adjustments to the system during this process is:

$$x'^j_i = \begin{cases} x'^j_i \pm bw \text{ with probability } PAR \\ x'^j_i \text{ with probability 1-}PAR \end{cases} \tag{3}$$

The system uses x and x' to show design parameters from the starting and updated hypothesis models. Parallel to genetic algorithm mutation this tool is known as PAR and adjusts value placement inside the database. This method determines change possibilities through the formula of HMCR and PAR The effectiveness of HS depends mainly on HMS, HMCR, PAR, bw, and NI settings. The HMS sets the boundaries where the HS algorithm looks for solutions. During step 2 the generated HM parameters get fine-tuned through the HMCR-PAR-bw process.

4-Updating harmony memory: When the new objective function f(x') gives higher value than f(x) the algorithm updates harmony memory by replacing the least effective design vector with this improved solution.

5-Checking the stopping criteria: The process combines these steps 3 and 4 until reaching all preset HS algorithm limits or finding the best result.

The rules for HMCR-PAR and bw remain fixed during each iteration of HS's ordinary function. Ultrasound inspection relies on proper parameter selection to work well because HS needs more time to find perfect answers according to Ouyang *et al*. (2015). The performance of HS has improved through various enhanced methods to achieve better optimization results faster. Mahdavi *et al*. (2007) developed an Updated Harmony Search approach that automatically changes the settings of PAR and bwbw to optimize performance. The rules for HMCR-PAR and bwbw remain fixed during each iteration of HS's ordinary function. Ultrasound inspection relies on proper parameter selection to work well because HS needs more time to find perfect answers according to Ouyang *et al*. (2015). The performance of HS has improved through various enhanced methods to achieve better optimization results faster. Mahdavi *et al*. (2007) developed an updated harmony search approach that automatically changes the settings of PAR and bw to optimize performance as:

$$PAR(k) = PAR_{\min} + \frac{PAR_{\max} - PAR_{\min}}{NI} k \tag{4}$$

$$bw(k) = bw_{\max} \exp[\frac{Ln(bw_{\min}) - Ln(bw_{\max})}{NI} k] \tag{5}$$

in which, PAR_{min} and PAR_{max} are the min and max values of the adjusting pitch rate, respectively. $PAR(k)$ denotes the pitch considered adjusting rate for the k_{th} generation.

The process of improvisation in the IHS works like the basic HS algorithm. However, IHS often performs better than HS when tackling optimization problems. In 2008, Omran and Mahdavi came up with the GHS algorithm. This GHS approach uses *PAR(k)*, which is shown in Eq. (4), and it relies on the best harmony memory available. In GHS, the adjustment pitch step used in HS is updated by incorporating the best harmony memory during the improvisation stage.

$$x'^j_i = \begin{cases} x_i^{best} \text{ with probability } PAR(k) \\ x'^j_i \text{ with probability 1-}PAR(k) \end{cases} \tag{6}$$

in which, x^{best} denotes the best HM in the memory.

The IHM may be enhanced for better global optimization by using a process that changes over time. The AAHS optimization algorithm is introduced, featuring two stages of adjustment and incorporating the GHS. At the first step of AAHS, the HM is adjusted with a dynamic bandwidth and a changing Harmony Memory Considering Rate (HMCR). In the 2nd step, a new HM is fine-tuned. The AAHS introduces a variable HMCR as:

$$HMCR(k) = 0.95 + 0.1 \times \sqrt{\frac{k}{NI} - (\frac{k}{NI})^2} \tag{7}$$

in which, k denotes the iteration number, *NI* denotes the total number of improvisations. The dynamic bandwidth may be written as:

$$Bw(k) = \frac{x}{{}^{10}_{max^{min}} exp[-10\frac{k}{NI}]} \tag{8}$$

in which, x^{max} and x^{min} present the max and min design variables, respectively. The new HM is:

$$x' = x + (2 \times rand() - 1) \times Bw(k) \quad (9)$$

To determine the bandwidth of dynamic for each design variable, we use a logarithmic function. This function considers the highest and lowest values found in the harmony memory (HM), which come from Eq. (8) during each step. As we keep optimizing, the logarithmic function makes the bandwidth get smaller. This results in a very narrow bandwidth in the later stages of optimization. After narrowing the bandwidth, we adjust the new harmony memory (HM) with something called the dynamic pitch adjustment rate, written as PAR(k). We use a specific formula for this adjustment. This process helps make the harmony memory better with each iteration:

$$PAR(k) = 0.3 + 0.6 \times [1 - \sqrt{1 - k/NI}] \quad (10)$$

The new adjustment is:

$$x' = x' + (2 \times rand() - 1) \times \alpha(k) \quad [x^{max^{min}} \quad (11)$$

in which α denotes a step size as:

$$\alpha(k) = \sqrt{1 - k/NI} \quad (12)$$

To find the best direction for each variable, we start by using the values in the HM. These values help us change the HM by looking at the difference between the highest and lowest values. In Eq. (11), there's a part that creates a random bandwidth that's always more than zero. This helps us fine-tune the HM. We change each HM from its old state using the step size mentioned in Eq. (12). Initially, this step size is large, which allows for wide changes in the design variables. The harmony memory is adjusted based on a probability of HMCR(k) × PAR(k) using a changing step size and bandwidth. As a result, the AAHS method might reduce the number of best local solutions in problems with many possible best solutions. Starting with the initial harmony memory, the AAHS can be updated in three random ways: 1) by using the old HM members and adjusting them with a changing bandwidth, 2) by changing the new HM based on the old HM's statistics, 3) by randomly picking each memory member from the available options.

The way AAHS adjusts things is not the same as the original HS, IHS, and GHS methods. It creates a new HM through two steps that look at the old harmony memory's stats (the gap between the highest and lowest values for each design variable in the old HM). This approach figures out its settings on its own, with the main ones being the HMS and NI.

3. Modelling of structure

A beam, which is made with a length L, and a cross-sectional area of b*h, is shown in Fig. 1. A voltage applied in the thickness direction is used to induce the electrostatic effects within the material, thus, it affects the mechanical

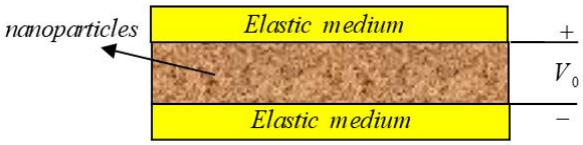

Fig. 1 The schematic of the beam with smart nanoparticles in elastic medium

properties. The beam is additionally supported by an elastic foundation, which in turn provides extra constraints and flexibility to the structure. The interaction and coupling between reproducing the nanoparticle reinforcement and the voltage source cause changes in the beam deformation, stress distribution, and the overall dynamic behavior of the beam.

The incorporation of smart nanoparticles is responsible for the material to acquire piezoelectric properties which permit the connection of mechanical and electrical behaviors. In this nanocomposite material, the stress (σ) and strain (ε) in the structure are mainly the results of the mechanical loading and the electrical displacement (D) that are generated by the applied electric field (E). This interaction occurs because of the piezoelectric properties of smart nanoparticles, in which the stress and strain are not only produced by external forces but also because of the interaction with the electric field that causes the electric polarization inside the material. The piezoelectric impact of the nanocomposite beam can lead to a convertible transformation that is between mechanical and electrical energy with the strain and stress representing the mechanical forces on the material and the voltage-induced electric fields. This exclusive association between the electrical and mechanical states of the material is indeed a vital component in the formation of smart structures and devices, where both sensing and actuation capabilities are included in the same system. The basic relations are:

$$\begin{bmatrix}\sigma_{xx}\\ \sigma_{yy}\\ \sigma_{zz}\\ \tau_{yz}\\ \tau_{xz}\\ \tau_{xy}\end{bmatrix} = \begin{bmatrix}C_{11} & C_{12} & C_{13} & 0 & 0 & 0\\ C_{12} & C_{22} & C_{23} & 0 & 0 & 0\\ C_{13} & C_{23} & C_{33} & 0 & 0 & 0\\ 0 & 0 & 0 & C_{44} & 0 & 0\\ 0 & 0 & 0 & 0 & C_{55} & 0\\ 0 & 0 & 0 & 0 & 0 & C_{66}\end{bmatrix} \begin{Bmatrix}\varepsilon_{xx}\\ \varepsilon_{yy}\\ \varepsilon_{zz}\\ \gamma_{yz}\\ \gamma_{xz}\\ \gamma_{xy}\end{Bmatrix} - \begin{bmatrix}0 & 0 & e_{31}\\ 0 & 0 & e_{32}\\ 0 & 0 & e_{33}\\ 0 & e_{24} & 0\\ e_{15} & 0 & 0\\ 0 & 0 & 0\end{bmatrix} \begin{Bmatrix}E_x\\ E_y\\ E_z\end{Bmatrix}, \quad (13)$$

$$\begin{bmatrix}D_x\\ D_y\\ D_z\end{bmatrix} = \begin{bmatrix}0 & 0 & 0 & 0 & e_{15} & 0\\ 0 & 0 & 0 & e_{24} & 0 & 0\\ e_{31} & e_{32} & e_{33} & 0 & 0 & 0\end{bmatrix} \begin{Bmatrix}\varepsilon_{xx}\\ \varepsilon_{yy}\\ \varepsilon_{zz}\\ \gamma_{yz}\\ \gamma_{xz}\\ \gamma_{xy}\end{Bmatrix} + \begin{bmatrix}\in_{11} & 0 & 0\\ 0 & \in_{22} & 0\\ 0 & 0 & \in_{33}\end{bmatrix} \begin{Bmatrix}E_x\\ E_y\\ E_z\end{Bmatrix}, \quad (14)$$

in which C_{ij}, e_{ij} and $\in_{ij}$ denote elastic, piezoelectric

and dielectric constants, respectively. The electric field (E_k) is:

$$E_k = -\nabla\Phi, \tag{15}$$

where:

$$\Phi(x,z,t) = -cos\left(\frac{\pi z}{h}\right)\varphi(x,t) + \frac{2V_0 z}{h} \tag{16}$$

here V_0 denotes the voltage. Now, based on SSDT (Thai and Vo 2012), we have:

$$\begin{aligned}\sigma_{xx} &= C_{11}\left(\frac{\partial u}{\partial x} - z\frac{\partial^2 w}{\partial x^2} + \frac{h}{\pi}sin\left(\frac{\pi z}{h}\right)\frac{\partial\psi}{\partial x}\right)\\ &+e_{31}\left(\frac{\pi}{h}sin\left(\frac{\pi z}{h}\right)\phi + \frac{2V_0}{h}\right).\end{aligned} \tag{17}$$

$$\sigma_{xz} = C_{55}\left(cos\left(\frac{\pi z}{h}\right)\psi\right) - e_{15}\left(cos\left(\frac{\pi z}{h}\right)\frac{\partial\phi}{\partial x}\right), \tag{18}$$

$$D_x = e_{15}\left(cos\left(\frac{\pi z}{h}\right)\psi\right) + \in_{11}\left(cos\left(\frac{\pi z}{h}\right)\frac{\partial\phi}{\partial x}\right), \tag{19}$$

$$\begin{aligned}D_z &= e_{31}\left(\frac{\partial u}{\partial x} - z\frac{\partial^2 w}{\partial x^2} + \frac{h}{\pi}sin\left(\frac{\pi z}{h}\right)\frac{\partial\psi}{\partial x}\right)\\ &-\in_{33}\left(\frac{\pi}{h}sin\left(\frac{\pi z}{h}\right)\phi + \frac{2V_0}{h}\right),\end{aligned} \tag{20}$$

here u and w present the displacements and ψ is rotation. It's important to understand that for solid materials, we can determine their mechanical and electrical properties using a model called the micro-electro-mechanical system (MEMS). Tang and Tong demonstrated this in 2001. This approach allows us to closely examine the interaction between mechanical and electrical behaviors in materials, especially those with the piezoelectric effect, such as ZnO nano-particles. The MEMS model helps researchers analyze how mechanical stresses and strains interact with electrical fields in composite materials. By using this model, we can explore how structural changes cause the production and distribution of electric fields. It also serves as a valuable tool for improving smart materials and devices. The method provides insights into how materials respond under various conditions, enhancing the accuracy of models for applications like sensing, actuation, and energy harvesting systems. The potential energy and external work are:

$$U = \frac{1}{2}\int_V \begin{pmatrix}\sigma_{xx}\left(\frac{\partial u}{\partial x} - z\frac{\partial^2 w}{\partial x^2} + \frac{h}{\pi}sin\left(\frac{\pi z}{h}\right)\frac{\partial\psi}{\partial x}\right)\\ +\sigma_{xz}\left(cos\left(\frac{\pi z}{h}\right)\psi\right) - D_x\left(cos\left(\frac{\pi z}{h}\right)\frac{\partial\phi}{\partial x}\right)\\ -D_z\left(-\frac{\pi}{h}sin\left(\frac{\pi z}{h}\right)\phi - \frac{2V_0}{h}\right)\end{pmatrix} dV \tag{21}$$

$$W = \int_x \left(-k_w w + k_g\nabla^2 w\right)w dx. \tag{22}$$

here k_w and k_g respectively denote spring and shear coefficients. In final, based on Hamilton's principle, we have:

$$\delta u: \frac{\partial^2 u}{\partial x^2} + \frac{\partial w}{\partial x}\frac{\partial^2 w}{\partial x^2} = 0, \tag{23}$$

$$\begin{aligned}\delta w: &-C_{11}I\frac{\partial^4 w}{\partial x^4} + \frac{24C_{11}I}{\pi^3}\frac{\partial^3\psi}{\partial x^3}\\ &-(2e_{31}V_0 + N_x^M)\frac{\partial^2 w}{\partial x^2} - k_w w + k_g\nabla^2 w = 0,\end{aligned} \tag{24}$$

$$\begin{aligned}\delta\psi: &-\frac{24C_{11}I}{\pi^3}\frac{\partial^3 w}{\partial x^3} + \frac{6C_{11}I}{\pi^2}\frac{\partial^2\psi}{\partial x^2}\\ &+\frac{e_{31}h}{2}\frac{\partial\phi}{\partial x} - \frac{Q_{55}A}{2}\psi + \frac{e_{15}h}{2}\frac{\partial\phi}{\partial x} = 0,\end{aligned} \tag{25}$$

$$\begin{aligned}\delta\phi: &-\frac{2h}{\pi}\frac{\partial^2 w}{\partial x^2} + \frac{h}{2}\frac{\partial\psi}{\partial x} - \frac{\pi^2\in_{33}}{2h}\phi\\ &+\frac{h}{2}\frac{\partial\psi}{\partial x} + \frac{h\in_{11}}{2}\frac{\partial^2\phi}{\partial x^2} = 0.\end{aligned} \tag{26}$$

where N_x^M is the axial force. The above equations in matrix form are:

$$\left([K] + P\left[K_g\right]\right)\{d\} = 0 \tag{27}$$

where P denotes the buckling load, $[K_g]$, $[K]$ and $[d]$ respectively, are the geometric matrix, stiffness matrix and deflection vector.

An easy way to find the critical buckling load of a nanocomposite sinusoidal structure is by solving the eigenvalue problem. This is a simple method used for structural stability analysis. In this process, we investigate how the structure reacts to applied loads by using the main equations of motion. We usually include a combination of elasticity theory and structural mechanics in this work. The eigenvalue problem can aid us in the determination of the natural frequencies and mode shapes of the structure, which are important in the detection of whether the structure shall fail under a certain load. We get this from finding solution for this problem which tells us the critical buckling load, beyond that the systems lose stability and deform suddenly. On nanocomposite sinusoidal structures, this analysis can be done based on physical properties such as how the nanoparticles toughen the material and geometrical factors. A more accurate prediction of buckling behavior under different conditions is possible with this type of analysis. This technique is effective in the case of optimizing the design of lightweight, high-performance nanocomposite structures where stability and bearing load are predominant.

4. Results and discussions

A cloud-based system performed optimization analysis for nanocomposite beams containing smart nanoparticles and produced valuable results about their structural strength. Under 50 GPa restraint and an applied 100 V voltage the analysis discovered its best structural outcome.

We need to verify the buckling results reported here through this work. In order to compare our results a simple beam buckling test is performed omitting the ZnO nanoparticles ($rho = 0$), support layers ($k_w = k_g = 0$) and piezoelectric effects of the system. With comparable material specifications and geometric data as Thai and Vo (2012), this research shows beam buckling results in Table 1 for multiple length-to-thickness ratios. The study results

Table 1 Validation of this paper with (Thai and Vo 2012)

L/h	TBT, (Thai and Vo 2012)	SSDT, (Thai and Vo 2012)	SSDT, present
5	8.9509	8.9533	8.9533
10	9.6227	9.6232	9.6232
20	9.8067	9.8068	9.8069
100	9.8671	9.8671	9.8673

Table 2 Evaluate several harmony optimization methods for best result selection from nanocomposite beam data

Variable	HS	IHS	GHS	AAHS
L (nm)	0.2688	0.2499	0.2389	0.21817
h (nm)	0.044	0.046	0.0552	0.0493
rho	0.048	0.052	0.0503	0.055
kw (N/m^2)	115×10^9	127×10^9	133×10^9	118×10^9
kg (N/m^2)	27.33	29.17	20.23	29
Cost ($)	59.87	55.21	60.17	45.78

show close agreement with the findings of Thai and Vo (2012) which validates our research.

4.1 Optimization results

This section tests four harmony search methods HS, IHS, GHS and AAHS using a single voltage value V0=100 volte under conditions of hollow and upper foundation property bounds and spring-shear constants, and 10 memory slots with 5000 improvisations each. Our study uses HMCR=0.97 for all harmony searches and sets bw to (xmax-xmin)/100, PAR to 0.29 for HS, and PARmin=0.12, bwmax=(xmax-xmin)/20, bwmin=0.002, PARmax=0.93 for IHS and GHS according to Keshtegar *et al.* (2017). This method changes its performance settings with every processing cycle. Our research group examines the optimal solutions for this complex design applying the HS, IHS, GHS, and AAHS methods in Section 4 and lists their results in Table 2.

Our findings in Table 2 confirm that harmony search optimization tools produce good solutions for our nanocomposite design problem. By using IHS we achieve better outcomes than HS and GHS yet AAHS delivers maximized accuracy improvement of 17% for our IHS results. Our AAHS system produces the best possible solution among the HS, IHS, and GHS designs at Cost= 45.78$. GHS provides the most effective solution results among other harmony search methods with nanocomposite beam designs. The AAHS shows better results than IHS. This algorithm finds superior results than all other harmony search methods worldwide. AAHS requires better adjustment procedures by letting HS use dynamic parameters to better modify the harmony memory. The optimal design created from AAHS shows (0.21817 m, 0.0493 m, 118 GPa, 29 Pa, 0.055) as output while achieving a budget of 45.78 dollars. In this situation the end results reach their bottom boundary levels and deliver their best values for foundation springs and shear constants. The thickness of beam h and the amount of zinc oxide nanoparticles rho influence the cost values more than they do the buckling force of nanocomposite beams.

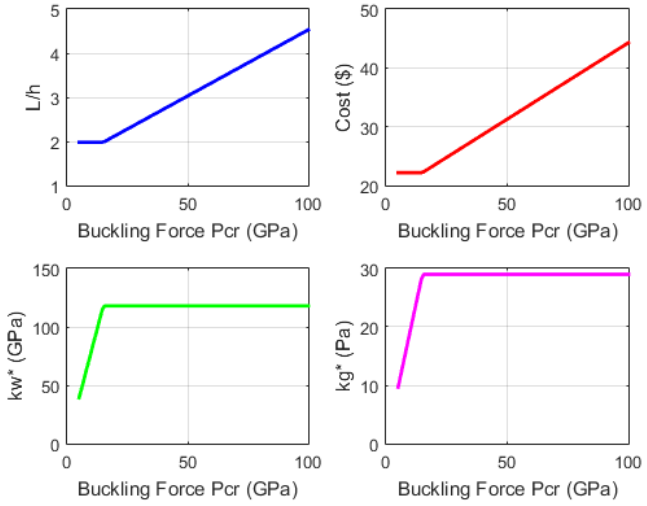

Fig. 2 AAHS algorithm examines forces from bucking constraints to determine the effect on four design parameters including length to thickness ratio optimization and cost reduction analysis followed by foundation spring constant optimization and foundation shear optimization

Based on the optimization model in Eq. (30), Fig. 2 shows the proper design of *L/h* ratio and cost alongside foundation spring and shear constants at multiple buckling loads under 100 volte voltage. (30) with applied voltage of 100 volte. The application uses 118 GPa as the maximum value for spring constant (*kw*) and 29 Pa as the maximum value for shear constant (*kg*) of foundation. The optimized ZnO nanoparticle volume fraction reached 0.055 during all optimization processes that employed multiple applied constraint values. The *L/h* length-to-thickness ratio and 45.78 $ cost remain consistent while spring constant and shear constant of foundation increase proportionally between Pcr = 0 to Pcr = 15 GPa. The study demonstrates that the spring constant and shear constant reach their maximum values during 15-100 GPa for applied buckling forces with spring constant at 118 GPa and shear constant equal to 29 Pa. The nanocomposite beam experiences a nonlinear increase in *L/h* ratio and cost values while Pcr values rise between 15 and 100 GPa. An increase in the nanocomposite beam cost occurs after Pcr exceeds the threshold of 15 GPa. By increasing the nanocomposite beam length one can enhance its elastic functional strength through the application of an optimal spring constant kw = 118 GPa.

4.2 Impacts of various parameters

Using an optimization model with Pcr force of 50 GPa and 100 volte applied voltage the research analyzes how ZnO nanoparticle volume fraction (rho) affects the results for foundation stiffness coefficients ranging from 50 to 200 to 150 to 200 GPa. The cost data and length to thickness ratio variations of the nanocomposite beam are demonstrated in Figs. 3 and 4, respectively based on four different foundation spring and shear constants settings. When adding

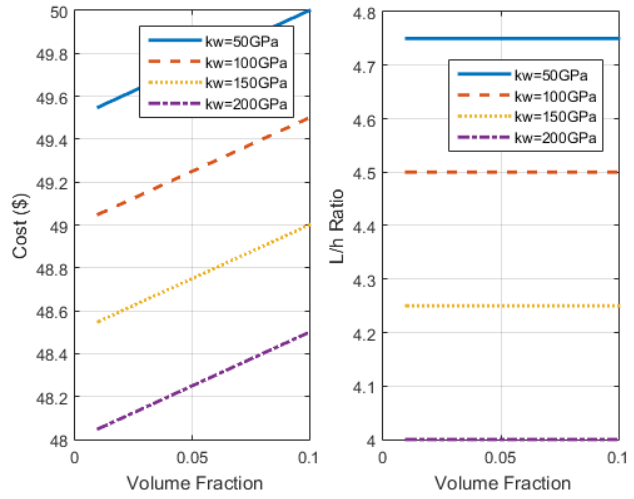

Fig. 3 The impact of spring constant on the cost and optimum *L/h*

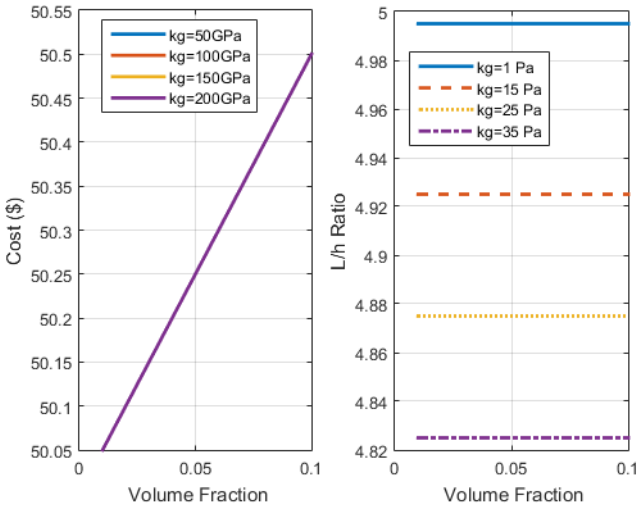

Fig. 4 The impact of shear constant on the cost and optimum L/h

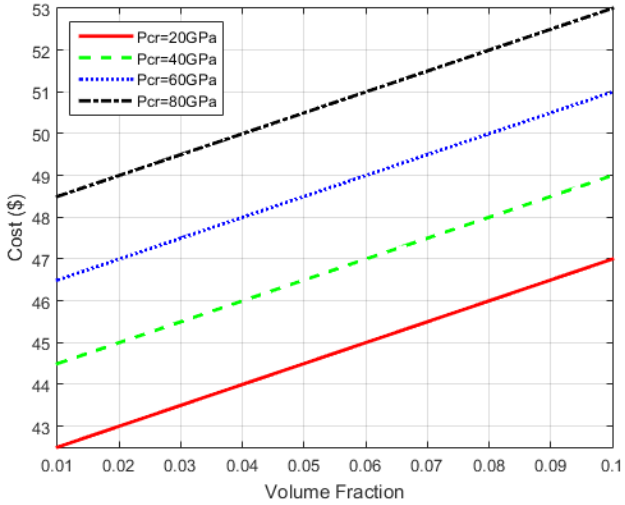

Fig. 5 The impact of buckling forces on the cost

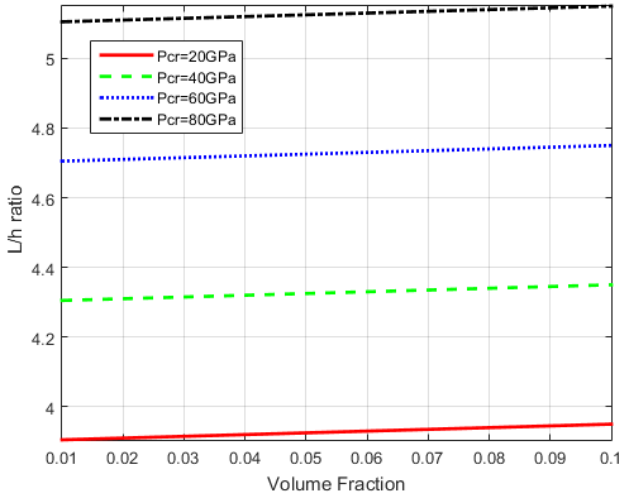

Fig. 6 The impact of buckling forces on the optimum *L/h*

greater amounts of ZnO nanoparticles the cost function of structure elevates since it requires more nanoparticle materials. The study shows that foundation spring constant has minor impact on selecting different L/h ratios under various kw conditions. The structure cost decreases together with the optimal L/h ratio when foundation spring constants become higher. When foundation shear constant increases the cost function remains unchanged but foundation cost changes. The stiffness of the structure enhances as kw and kg become larger which leads to enhanced buckling load and finally lower L/h optimum value. As the optimum value of L/h decreases the required construction materials decrease which requires lower cost expenditures.

The variations in cost and optimum length-to-thickness ratio (L/h) of the nanocomposite beam are presented in Figs. 5 and 6 according to different volume fractions of ZnO nanoparticles (ρ) under applied buckling loads of 20, 40, 60, and 80 GPa. The optimization model produces result by utilizing an applied voltage of 100 volts together with an upper stiffness constant of 118 GPa and an upper shear constant of 29 Pa for the foundation. Both the structural cost and optimal L/h ratio rise when critical buckling load increases according to the presented figures. An increase in critical buckling load typically reduces structural stiffness which requires more L/h ratio to ensure stability of the structure. The extended beam proportions compared to its dimensions need additional materials leading to elevated overall expenses. The evaluation demonstrates the important role that ZnO nanoparticle reinforcement plays during the optimization procedures. The addition of ZnO nanoparticles to enhance the nanocomposite beam properties produces higher costs because these nano-particles have a more expensive price than conventional materials. The changes in ρ produce minor variations in L/h optimal ratio compared to the changes in the buckling load parameters. The findings establish that ZnO nanoparticle reinforcement enhances mechanical performance yet demands cost evaluation when assessing structural modifications especially under high buckling loads. Through optimization methods designers obtain essential information about picking right design criteria which strikes performance quality off against cost-effectiveness requirements for nanocomposite beams.

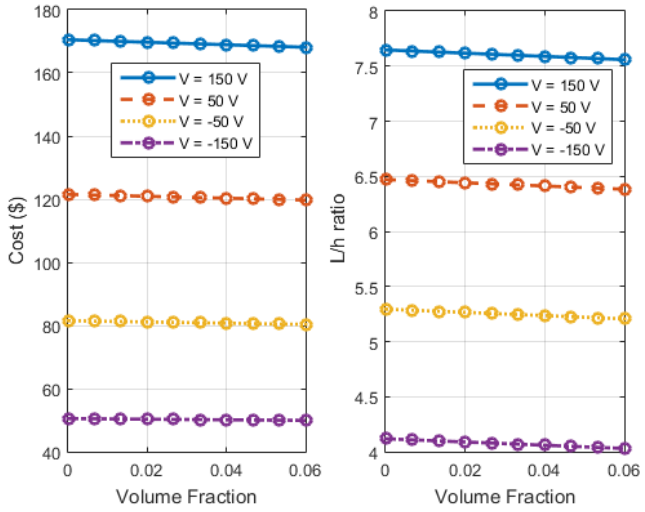

Fig. 7 The impact of voltages on the cost and optimum *L/h*

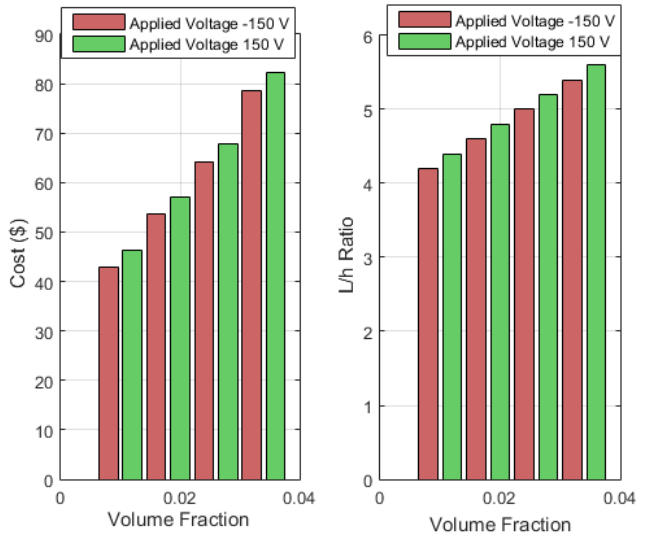

Fig. 8 The impact of voltages and volume fraction on the cost and optimum *L/h*

Fig. 7 establishes how the nanocomposite beam's structural performance and cost factors link together with the applied voltage and ZnO nanoparticle volume fraction. Changes in ZnO nanoparticle volume fractions do not influence how the beam behaves mechanically when measured by its L/h optimum ratio. The increasing amount of ZnO nanoparticles in the material leads to greater manufacturing expenses resulting from their higher material prices. Among the three fixed constants Pcr at 50 GPa and upper stiffness of 118 GPa and upper shear at 29 Pa which impact the beam performance, the applied voltage stands as the leading factor that determines the optimum L/h ratio. Portions of the beam develop greater rigidity due to their alignment under a negative voltage field allowing for both lower L/hL/h ratio selection and cost reduction of the entire system. Under specific loading conditions the beam becomes more efficient and stable because of this modification.

When utilizing positive external voltage across the beam a tensile stress develops which causes the nanocomposite material stiffness to decrease. The improvement in L/h L/h ratio combined with increased expense of production arises from larger dimensions required for structural support. The results indicate the ZnO content influences the L/hL/h ratio only marginally but the external voltage has a substantial effect on this value. When voltages remain at negative levels the material performance becomes stronger but costs stay lower yet when voltages turn positive structural modifications create higher costs. External voltage applications show a trade-off between stiffness and optimal design and cost because negative voltages improve performance but need greater design changes from positive voltage applications.

The optimization analysis for the nanocomposite beam displayed results through Fig. 8 which presented both manufacturing cost and optimal L/h ratio data at various ZnO nanoparticle volume fractions and applied voltages. The left subplot reveals that increasing ZnO nanoparticle volume fraction raises manufacturing costs because multiple nanoparticles require additional materials during production. The costs of production remain higher when applying 150 V compared to -150 V but show the same upward pattern for both voltage values because the structural design gets more intricate with each additional voltage. The performance benefits from adding ZnO nanoparticles have implications for increased material costs which requires optimization of the cost-volume fraction relationship.

The right subplot of Fig. 9 displays the optimum L/h ratio for the nanocomposite beam as a function of the ZnO nanoparticle volume fraction and applied voltage. The structural stability requirement with ZnO nanoparticles becomes higher as their volume fraction increases because these nanoparticles improve the beam properties. The L/h ratio changes when an electric field with various applied voltages is used: A negative voltage (-150 V) decreases the L/h ratio while positive voltage (+150 V) leads to increased L/h ratio because tension develops within the structure. The beam exhibits a sensitive response to both its material composition through ZnO fraction and external voltage conditions because both factors need precise balancing for optimal performance.

5. Conclusions

The research experiment proves successful in illustrating how ZnO nanoparticles affect nanocomposite beam performance by showing how loads and voltage levels and foundation stiffness work together to reach optimal design outcomes. Research applications of advanced adaptive harmony search (AAHS) identifies 4.425 L/h ratio along with 118 GPa foundation spring constant together with 29 Pa shear constant in combination with 0.055 ZnO nanoparticle volume fraction as optimal design parameters for specific applied voltage and buckling force conditions. Through the optimization process using the AAHS algorithm the performance was enhanced while cutting manufacturing costs effectively since the algorithm delivered superior accuracy and results compared to traditional methods. The results show how system performance relates directly to the expenses involved when

adjusting ZnO nanoparticle volume fraction along with applied voltage values. Through greater nanoparticle addition there are better mechanical properties for the beam but production expenses increase substantially with elevated applied voltages. The analysis proves that negative voltage system strengthens the structural rigidity of the beam thus reducing the L/h proportion and lowering creation expenses yet positive voltage creates longer beams at elevated costs. The experimental findings demonstrate why it matters to find suitable equilibrium between these design elements for creating optimized cost-efficient and high-performance nanocomposite beams that serve diverse structural needs.

Nanocomposite reinforced sinusoidal beam design and optimization benefits substantially from the usage of adaptive improved harmony search (AAHS) due to its ability to produce better outcomes than traditional harmony search algorithms. The study identifies the three main influential variables applied voltage buckling constraint forces and foundation spring constant to create an optimization structure for the critical ratio L/h. Through such design performance engineers can create efficient nanocomposite beams that meet specific design requirements involving buckling resistance plus applied voltage limitations. The AAHS method provides future researchers with a dependable tool due to its robust performance and accuracy as they advance both composite materials and structural optimization.

References

Azadi, R. and Rostamiyan, Y. (2015), "Experimental and analytical study of buckling strength of new quaternary hybrid nanocomposite using Taguchi method for optimization", *Constr. Build. Mater.*, **88**, 212-224. https://doi.org/10.1016/j.conbuildmat.2015.04.018.

Alesadi, A., Galehdari, M. and Shojaee, S. (2017), "Free vibration and buckling analysis of cross-ply laminated composite plates using Carrera's unified formulation based on Isogeometric approach", *Comput. Struct.*, **183**, 38-47. https://doi.org/10.1016/j.compstruc.2017.01.013.

Berghouti, H., Adda Bedia, E., Benkhedda, A. and Tounsi, A. (2023), "Vibration analysis of nonlocal porous nanobeams made of functionally graded material", *Adv. Nano Res.*, **7**(5), 351-364. http://doi.org/10.12989/anr.2023.7.5.351.

Belarbi, M.O., Houari, M.S.A., Daikh, A.A., Garg, A., Merzouki, T., Chalak, H.D. and Hirane, H. (2021), "Nonlocal finite element model for the bending and buckling analysis of functionally graded nanobeams using a novel shear deformation theory", *Compos. Struct.*, **264**, 113712. https://doi.org/10.1016/j.compstruct.2021.113712.

Belarbi, M.O., Houari, M.S.A., Hirane, H., Daikh, A.A. and Bordas, S.P.A. (2022), "On the finite element analysis of functionally graded sandwich curved beams via a new refined higher order shear deformation theory", *Compos. Struct.*, **279**, 114715. https://doi.org/10.1016/j.compstruct.2021.114715.

Belarbi, M.O., Khechai, A., Houari, M.S.A., Bessaim, A., Hirane, H. and Garg, A. (2024), "Free vibration behavior of sandwich FGM beams: Parametric and uncertainty analysis", *J. Vib. Eng. Technol.*, **12**(5), 883-905. https://doi.org/10.1007/s42417-024-01452-7.

Belarbi, M.O., Benounas, S., Salami, S.J., Khechai, A., Daikh, A.A., Houari, M.S.A. and Bezzina, S. (2025), "An enhanced finite element model for static bending analysis of functionally graded plates with power-law, exponential, and sigmoid material gradients", *Arch. Appl. Mech.*, **95**, No. 25, 1-20. https://doi.org/10.1007/s00419-024-02727-x.

Belabed, Z., Houari, M.S.A., Tounsi, A., Mahmoud, S.R. and Bég, O.A. (2014), "An efficient and simple higher order shear and normal deformation theory for functionally graded material (FGM) plates", *Compos. Part B Eng.*, **60**, 274-283. https://doi.org/10.1016/j.compositesb.2013.12.057.

Cheng, H.C., Hsieh, K.Y. and Chen, K.M. (2011) "Thermal–mechanical optimization of a novel nanocomposite-film typed flip chip technology", *Microelect. Reliab.*, **51**, 826-836. https://doi.org/10.1016/j.microrel.2010.11.007.

Daikh, A.A., Drai, A., Bensaid, I., Houari, M.S.A. and Tounsi, A. (2021), "On vibration of functionally graded sandwich nano-plates in the thermal environment", *J. Sandw. Struct. Mater.*, **23**(6), 3027-3052. https://doi.org/10.1177/1099636220909790.

Daikh, A.A., Houari, M.S.A., Belarbi, M.O., Mohamed, S.A. and Eltaher, M.A. (2022), "Static and dynamic stability responses of multilayer functionally graded carbon nanotubes reinforced composite nanoplates via quasi 3D nonlocal strain gradient theory", *Def. Technol.*, **18**(10), 1778-1809. https://doi.org/10.1016/j.dt.2021.09.011.

Daikh, A.A., Belarbi, M.-O., Vinh, P.V., Li, L., Houari, M.S.A. and Eltaher, M.A. (2024), "Vibration analysis of tri-directionally coated plate via thickness-stretching and microstructure-dependent modeling", *Mech. Res. Commun.*, **135**, 104221. https://doi.org/10.1016/j.mechrescom.2023.104221.

Garg, A., Chalak, H.D., Zenkour, A.M., Belarbi, M.O. and Houari, M.S.A. (2022), "A review of available theories and methodologies for the analysis of nano isotropic, nano functionally graded, and CNT reinforced nanocomposite structures", *Arch. Comput. Methods Eng.*, **29**, 2237-2270. https://doi.org/10.1007/s11831-021-09652-0.

Horny, N., Kanake, Y., Chirtoc, M. and Tighzert, L. (2016), "Optimization of thermal and mechanical properties of bio-polymer based nanocomposites", *Polym. Degrad. Stab.*, **127**, 105-112. https://doi.org/10.1016/j.polymdegradstab.2016.01.006.

Kamarian, S., Shakeri, M. and Yas, M. (2018), "Natural frequency analysis and optimal design of CNT/fiber/polymer hybrid composites plates using mori-tanaka approach, GDQ technique, and firefly algorithm", *Polym. Compos.*, **39**(5), 1433-1446. https://doi.org/10.1002/pc.24083.

Khechai, A., Tounsi, A., Houari, M.S.A. and Adda Bedia, E.A. (2020), "A refined shear deformation theory for bending and free vibration analysis of functionally graded beams", *Steel Compos. Struct.*, **36**(6), 643-658. https://doi.org/10.12989/scs.2020.36.6.643.

Kuang, J., Liu, Z., Shocrah, M. (2024), "A method of music education for sound absorption and in-phase harmonics synchronization: Using surface coupling theory to couple nano-sheets in musical instruments", *Adv. Nano Res.*, **17**(6), 525-531. https://doi.org/10.12989/anr.2024.17.6.525.

Mansour, G., Tsongas, K. and Tzetzis, D. (2018), "Modal testing of nanocomposite materials through an optimization algorithm", *Measurement*, **91**, 31-38. https://doi.org/10.1016/j.measurement.2016.05.032.

Mahdavi, M., Fesanghary, M. and Damangir, E. (2007), "An improved harmony search algorithm for solving optimization problems", *Appl. Math. Comput.*, **188**, 1567-1579. https://doi.org/10.1016/j.amc.2006.11.033.

Merzouki, T., Houari, M.S.A., Bessaim, A., Haboussi, M., Dimitri, R. and Tornabene, F. (2022), "Bending analysis of functionally graded porous nanocomposite beams based on a non-local strain gradient theory", *Math. Mech. Solids.*, **27**(1), 3-26. https://doi.org/10.1177/10812865211011759.

Nejati, M., Eslampanah, A. and Najafizadeh, M. (2016), "Buckling

and vibration analysis of functionally graded carbon nanotube-reinforced beam under axial load", *Int. J. Appl. Mech.*, **8**, 1650008. https://doi.org/10.1142/S1758825116500083.

Ouyang, H.B., Gao, L.Q, Li, S., Kong, X.Y., Wang, Q. and Zou, D.X. (2017), "Improved Harmony Search Algorithm: LHS", *Appl. Soft Comput.*, **53**, 133-167. https://doi.org/10.1016/j.asoc.2016.12.042.

Omran, M.G. and Mahdavi, M. (2008), "Global-best harmony search", *Appl. Math. Comput.*, **198**, 643-656. https://doi.org/10.1016/j.amc.2007.09.004.

Rouhi, M. and Rais-Rohani, M. (2013), "Modeling and probabilistic design optimization of a nanofiber-enhanced composite cylinder for buckling", *Compos. Struct.*, **95**, 346-353. https://doi.org/10.1016/j.compstruct.2012.05.035.

Sabherwal, P., Belarbi, M.O., Raman, R., Garg, A., Li, L., Chalak, H.D., Houari, M.S.A. and Avcar, M. (2024), "Free vibration analysis of laminated sandwich plates using wavelet finite element method", *AIAA J.*, **62**(2), 1-12. https://doi.org/10.2514/1.J063364.

Thai, H-T. and Vo, T.P. (2012), "A nonlocal sinusoidal shear deformation beam theory with application to bending, buckling, and vibration of nanobeams", *Int. J. Eng. Sci.*, **54**, 58-66. https://doi.org/10.1016/j.ijengsci.2012.01.009.

Tan, P. and Tong, L. (2001), "Micro-electromechanics models for piezoelectric-fiber-reinforced composite materials", *Compos. Sci. Tech.*, **61**, 759-769. https://doi.org/10.1016/S0266-3538(01)00014-8.

Vodenitcharova, T. and Zhang, L. (2006), "Bending and local buckling of a nanocomposite beam reinforced by a single-walled carbon nanotube",*Int. J. solids Struct.*, **43**, 3006-3024. https://doi.org/10.1016/j.ijsolstr.2005.05.014.

Wang, Y., Guo, Z. and Wang, Y. (2017), "Enhanced harmony search with dual strategies and adaptive parameters", *Soft Comput.*, **21**, 4431-4445. https://doi.org/10.1007/s00500-017-2563-1.

Yas, M. and Samadi, N. (2012), "Free vibrations and buckling analysis of carbon nanotube-reinforced composite Timoshenko beams on elastic foundation", *Int. J. Press. Vess. Pip.*, **98**, 119-128. https://doi.org/10.1016/j.ijpvp.2012.07.012

Yang, J., Wu, H. and Kitipornchai, S. (2017), "Buckling and postbuckling of functionally graded multilayer graphene platelet- reinforced composite beams", *Compos. Struct.*, **161**, 111-118. https://doi.org/10.1016/j.compstruct.2016.11.048.

Zhang, L., Song, Z. and Liew, K. (2018), "Computation of aerothermoelastic properties and active flutter control of CNT reinforced functionally graded composite panels in supersonic airflow", *Comput. Meth. Appl. Mech. Eng.*, **300**, 427-441. https://doi.org/10.1016/j.cma.2015.11.029